ARTICLE

Optical and grain boundary potential characteristics of sulfurized BiFeO$_3$ thin films for photovoltaic applications

Seung Min Lee and Yong Soo Cho[*]

Sulfurized BiFeO$_3$ (BFO) thin films have been investigated with the purpose of reducing their band gap for photovoltaic applications. A strong dependence of the degree of sulfurization on structure and optical properties of the BFO thin films was observed. The sulfurization process substantially reduced the optical band gap from 2.83 eV for the reference sample to ~1.90 eV in a sample sulfurized at 200 °C, a temperature at which the BFO phase was still dominant. The existence of secondary Bi$_2$S$_3$ phase was found to be initiated from the film surface and became serious at higher temperatures. XPS analysis suggests potential Bi-Fe(III)-Fe(II)-S-O compounds as a result of the change of oxidation state of Fe with the progress of sulfurization. The sulfurized BFO film exhibited relatively higher positively charged grain boundaries than the reference film, suggesting its improved applicability in photovoltaic devices.

Introduction

Recently, ferroelectric materials have attracted great interest for photovoltaic applications because of their polarization-induced photovoltaic effect.[1-3] BiFeO$_3$ (BFO) has been one of the most intensively investigated materials for photovoltaic applications owing to its relatively low band gap of ~2.70 eV compared to those of other ferroelectric materials.[4,5] However, this band gap is still much larger than the ideal of 1.30–1.60 eV for absorbers in photovoltaic devices, meaning that BFO has a limited range of optical absorption.[6,7] Therefore, reducing this band gap is necessary to promote more broadband light absorption in the solar spectrum. There have been several attempts to modify the optical properties of BFO thin films. For example, Dong et al.[8] improved the optical absorption of BFO by applying uniaxial compression to engineer the electronic structures and optical absorption. The approach of doping has been attempted in various studies, including the doping of BFO thin films with Mn, Eu and Co cations,[9-11] but none of these studies yielded any significant decrease in the band gap. For example, Xu at al.[9] studied the optical properties of BiFe$_{1-x}$Mn$_x$O$_3$ thin films with various Mn contents and reported a resultant reduction of band gap from ~2.65 to ~2.55 eV. Liu et al. [11] have demonstrated a change in the band gap of BFO films from ~2.69 to ~2.50 eV by doping with Eu.

In the meantime, anion substitution approaches have been reported to modify the optical properties of other oxide thin films for various applications; these approaches have included the use of H, S or N.[12-15] It is known that the substitution of O

with less electronegative elements shifts the absorption edge toward a lower energy level and thus narrows the optical band gap.[15] For TiO$_2$ and PbTiO$_3$, substitution of O with S was reported to be beneficial in such band gap tuning.[14,15] However, thus far there has been no report on the incorporation of S in BFO thin films for any purpose.

In this work, we investigate the effect of sulfurization upon the structural, optical and grain boundary characteristics of BFO thin films, primarily for the purpose of reducing the band gap for photovoltaic applications. Also, the grain boundary potential of an absorber material is known to be critical in determining minority carrier collection and current pathway in photovoltaic cells,[16,17] but there has been no such consideration regarding BFO thin films. Herein we report positive increases in grain boundary potential when S is introduced into the BFO structure, and conclude a substantial reduction in band gap, down to ~1.90 eV, with unexpected phase evolution.

Experimental section

BFO thin films were deposited onto a fluorine-doped tin oxide (FTO)/glass substrate by means of spin coating. To prepare a common precursor solution, bismuth acetate and iron acetate were dissolved into a solvent containing 2-methoxyethanol and acetic acid. This solution contained a 5 mol% excess of Bi to compensate for the loss of Bi during firing. The final 0.35 M precursor solution was spin-coated onto the FTO/glass substrate. After each spin coating, the film was dried at 100 °C for 1 min and then pyrolyzed at 350 °C for 5 min. The deposition process was repeated 6 times to prepare a film ~250 nm thick. The deposited films were annealed at 600 °C for 10 min by rapid thermal annealing in ambient atmosphere. Sulfurization was then carried out at various temperatures

Department of Materials Science and Engineering, Yonsei University, Seoul 120-749, Korea. E-mail: ycho@yonsei.ac.kr; Fax:+82-2-312-5375; Tel:+82-2-2123-5848

between 150 and 400 °C for 3 min under a $N_2 + H_2S$ (5%) flow in a tubular furnace, using the gas flow rate of 10 sccm.

The structures of film samples were analyzed by means of X-ray diffractometry (XRD, Max-2500, Rigaku B) using a Cu Kα radiation source. Surface morphology of the films was imaged by field-emission scanning electron microscopy (JSM-7001F). Transmission electron microscopy (TEM, JEM-ARM-200F, Jeol) combined with energy dispersive spectroscopy (EDS, X-MaxN 80T, Oxford Instruments) was used to characterize the structure and composition of films at high magnifications. The film samples' optical transmissions and reflections were measured at room temperature over the spectral range of 200–1600 nm by UV-visible spectrophotometry (JASCOV 530). The valence states of selected elements were studied by X-ray photoelectron spectroscopy (XPS, K-alpha, Thermo VG) using an Al Kα radiation source (1486.6 eV). Kelvin probe force microscopy (KPFM) measurements were performed by atomic force microscopy (AFM, NanoscopeV Multimode), utilizing a Pt/Ir-coated Si cantilever. The contact potential difference was detected and used to build up a topographical image by applying an AC bias of 1 V at a second resonance frequency of 270 kHz in the cantilever.

Results and discussion

Fig. 1(a) shows the XRD patterns of the BFO thin films at different sulfurization temperatures of 150, 200, 300 and 400 °C, which are highlighted in the 2θ range of ~23° to 36° for better identification of each phase. The XRD patterns over a broader 2θ range are shown in Fig. S1 in the Supplementary Information. The patterns indicate that the polycrystalline BFO phase was the main phase, and that Bi_2S_3 was the secondary phase, with intensity depending on the sulfurization temperature. Namely, lower peak intensity of the BFO phase was found at high sulfurization temperatures, indicating suppression of the BFO crystallinity with accompanying precipitation of Bi_2S_3. Fig. 1(b) illustrates this process, showing the relative intensity of $I_{BiFeO3(110)}/(I_{BiFeO3(110)} + I_{Bi2S3(130)})$ versus sulfurization
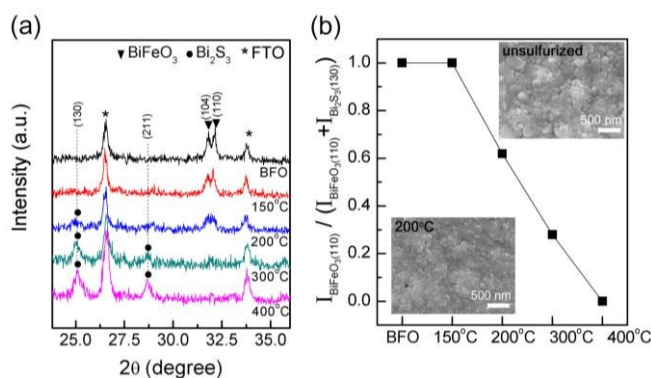
Fig. 1. (a) XRD patterns of unsulfurized and sulfurized BFO thin films at different sulfurization temperatures; (b) plot of the relative intensity of $I_{BiFeO3(110)}/(I_{BiFeO3(110)} + I_{Bi2S3(130)})$ versus sulfurization temperature. Selected surface microstructures of unsulfurized BFO film and a BFO film sulfurized at 200 °C are represented.

temperature. The two phases coexist only in the temperature range between 200 and 300 °C. The formation of the Bi_2S_3 phase is known to happen in the temperature range of 200–300 °C.[18] It should be noted that more intense sulfurization conditions, i. e., higher temperature (>300 °C) and longer reaction time (>10 min), resulted in the complete disappearance of crystalline BFO phase. The lattice constant of the BFO phase at 150 °C was calculated as 3.969 Å, slightly greater than the reference value of 3.961 Å; this may indicate the occupation of O sites by larger S ions.

Selected micrographs showing the surface microstructures of unsulfurized film samples and those sulfurized at 200 °C are shown in Fig. 1b. These micrographs show well-grown polycrystalline films with a relatively uniform distribution of grain size, most ranging between 100 and 200 nm. There was no large apparent difference in surface morphology before and after the sulfurization, although a slight decrease in grain size was observed.

TEM and EDS analyses were conducted on cross sections prepared using a standard focused ion beam (FIB) technique. A TEM image of the sample sulfurized at 200 °C shows a rough interface between the FTO and BFO layers due to the rough
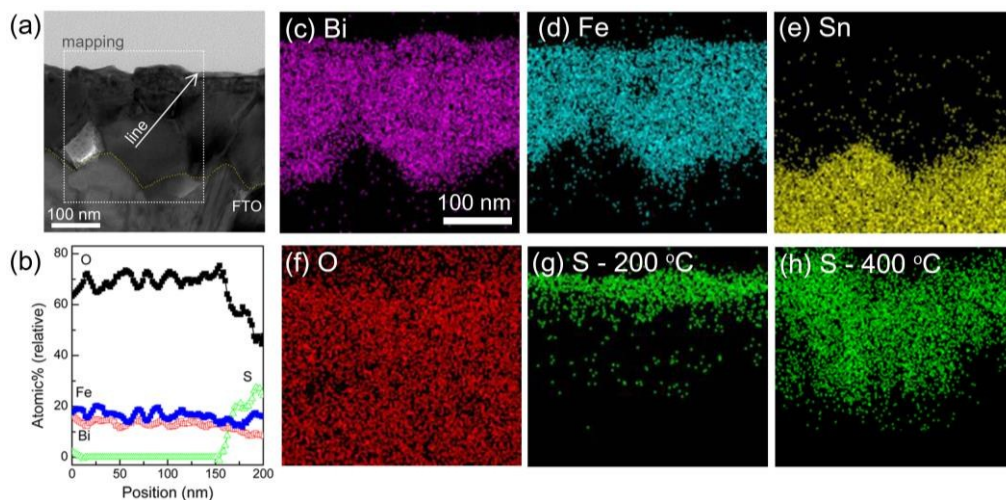
Fig. 2. (a) TEM image of sulfurized BFO at 200 °C and (b) EDS elemental line profiles taken along the direction of the arrows in the TEM image. (c–g) Elemental mapping results (at the same scale) for various elements in the BFO film sulfurized at 200 °C; (h) S mapping of a BFO film sulfurized at 400 °C.
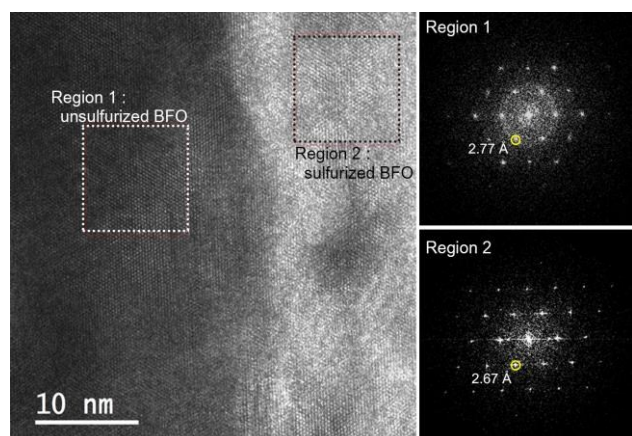
Fig. 3. HRTEM image of an interface between unsulfurized and sulfurized regions in 200 °C-sulfurized sample, with two electron diffraction patterns of each region.

FTO-coated substrate and distinct small grains are seen in the BFO films (Fig. 2(a)). An elemental line scan through the films implies that there was no distinguishable compositional change in S or O except in the ~50-nm-deep surface region of the film (Fig. 2(b)). In this surface region, there was a significant decrease in the relative O content compared to the inner region, with a subsequent increase of S content, suggesting that sulfurization starts from the surface.

To gain a detailed understanding of the elemental distribution in the sulfurized films, we also performed elemental mapping of the film sample sulfurized at 200 °C (Fig. 2(c)–(g)). The Sn mapping clearly showed the interface between the film and substrate (Fig. 2(e)). In the film, the distributions of the Bi and Fe components were uniform throughout the depth, showing no difference in color brightness; this matches the line profiles collected for Fe and Bi (Fig. 2(b)). Greater S concentration at the surface was again observed in this sample (Fig. 2(g)), but dispersed S (green dots in the figure) was observed in the interior of the film, indicating penetration of S at this temperature. The surface-initiated reaction of S was further evidenced by the observation of deeper S penetration in a sample sulfurized at the higher temperature of 400 °C (Fig. 2(h)). This observation indicates that the sulfurization progresses further from the surface in stronger sulfurization environments, such as at high temperatures.

Fig. 3 shows a high resolution TEM image representing an interface between the unsulfurized and sulfurized regions of the 200°C-sulfurized sample, with two FFT (fast Fourier transformed) electron diffraction patterns of the regions. From the comparison in the patterns, the decrease of d-spacing value from 2.77 Å (marked with a circle, (110) plane) to 2.67 Å was observed after sulfurization process. The decreased d-spacing also suggests the substitution of oxygen by sulfur with a larger ionic radius than that of oxygen. There have been numerous reports on the sulfurization of other absorber materials, such as $CuInSe_2$ and $Cu_2ZnSnSe_4$.[19-22] Keranen et al.[19] reported $CuInSe_2$ films sulfurized by means of a rapid thermal process in a H_2S/argon atmosphere. They reported that, at low
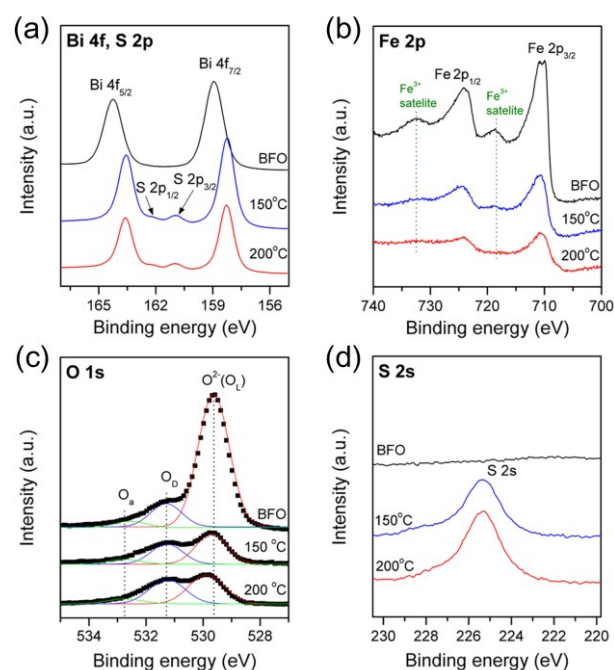
Fig. 4. XPS spectra of unsulfurized and sulfurized BFO thin films in the binding energy regions corresponding to (a) Bi 4f and S 2p, (b) Fe 2p, (c) O 1s, and (d) S 2s peaks with sulfurization temperature.

temperatures, S reacted only at the surface of the absorber. In a $Cu_2ZnSn(S,Se)_4$ absorber sulfurized from $Cu_2ZnSnSe_4$ films, a secondary phase of Cu_2S has been observed after sulfurization.[20]

Detailed XPS analysis was carried out to investigate the chemical states of elements in the sulfurized film surfaces (Fig. 4). Note that the XPS results correspond only to the surface region, up to the depth of ~10 nm. Two primary peaks at ~159.0 and ~164.3 eV were observed for BFO (Fig. 4(a)); these originate respectively from the binding energies for Bi $4f_{7/2}$ and Bi $4f_{5/2}$, with the spin orbital splitting energy of ~5.3 eV, which is in good agreement with reported energy values.[23] Low-intensity S $2p_{1/2}$ and S $2p_{3/2}$ peaks were also observed at ~162.1 and ~160.8 eV after sulfurization. The two Bi 4f peaks shifted to lower binding energy after sulfurization. The considerable shifts observed in the Bi 4f peaks were assumed to be associated with the formation of Bi-S bonds at the top surface of the sample, as shown in Fig. 2. This result matches with the XPS spectrum of Bi-S bonds reported by Fang et al.[24]

The XPS results showed a Fe 2p doublet consisting of a Fe $2p_{3/2}$ peak at ~710.6 eV and a Fe $2p_{1/2}$ peak at ~723.9 eV, which were attributed to Fe–O bonds (Fig. 4(b)). The spin-orbit splitting energy of the pure Fe 2p doublet was 13.3 eV, which is comparable to the theoretical value of 13.6 eV for Fe_2O_3.[25] It should be noted that satellite peaks were found 8 eV higher than the $2p_{3/2}$ peak, indicating the 3+ oxidation state of Fe.[26] Close examination of Fe 2p orbit was carried out through the peak fitting analysis, which reveals the coexistence of Fe^{2+} and Fe^{3+} in the both unsulfurized and sulfurized BFO thin films as shown in Fig. S2 of the Supplementary Information. Compared with unsulfurized film, it seems that the sulfurization induced the change of oxidation state of Fe. According to the ratio of
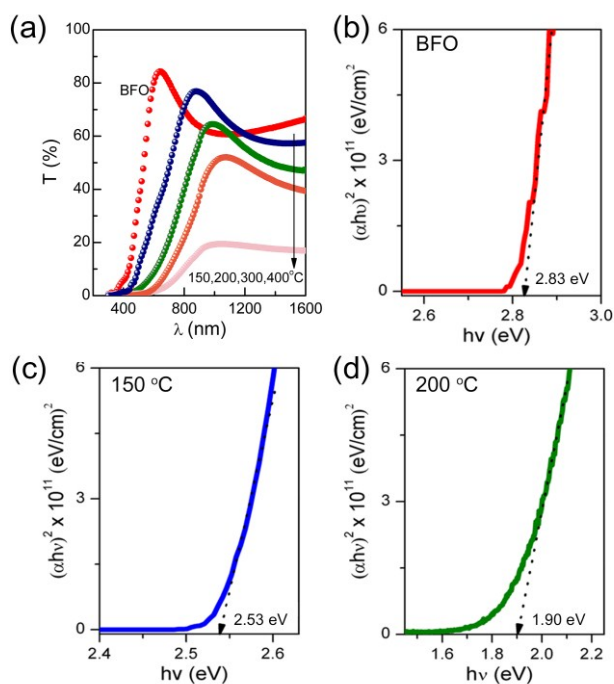
Fig. 5. (a) UV-visible transmittance spectra of films, and $(\alpha h\nu)^2$ vs $h\nu$ curves of (b) unsulfurized and sulfurized BFO thin films at (c) 150 ^{o}C and (d) 200 ^{o}C.

Fig. 6. (a–b) Spatial maps of surface potential on (a) the unsulfurized reference film and (b) the film sulfurized at 150 °C; brighter areas indicate higher electrochemical potentials. (c–d) Variations in surface potential along the lines shown in (a) and (b), respectively.

the fitted peak areas for Fe^{3+} and Fe^{2+}, concentration ratios of Fe^{3+} and Fe^{2+} in the BFO, 150 ^{o}C and 200 ^{o}C films are 89:11, 82:18 and 76:24, respectively. It indicates that H_2S reduces the oxidation state of Fe ions during annealing. It is very likely that the complex Bi-Fe(III)-Fe(II)-S-O compounds form as a result of the sulfurization process even the exact composition is difficult to be identified.

Asymmetric and broad peaks were observed in the O 1s spectrum (Fig. 4(c)); these were resolved into three distinct peaks positioned at ~529.6, 531.4 and 532.8 eV, and were then attributed to three different O species. Respectively, these species were O^{2-} ions (O_L) participating in Bi–O bonds in the perovskite; O defects (O_D); and absorbed O (O_a) in weakly bonded O species such as $-CO_3$ and $-OH$.[26] Significant decreases in the intensity of the O_L peak at ~529.6 eV were observed in the surface layer after sulfurization; thus the O_L/O_D ratio was remarkably reduced compared to the unsulfurized reference film. It is interesting to note that the defect levels were unchanged by the sulfurization. It is likely that the high concentration of O deficiencies caused by anion substitutions increases the concentration of defect states in the valence band edge, thereby widening the valence band and thus contributing to narrowing of the band gap.[27] In addition, the appearance of the S 2s peak after sulfurization also confirms the incorporation of S at the surface (Fig. 4(d)). Additional XPS spectra showing the depth profiles, which were obtained by Ar^+ sputter etching, can be seen in Fig. S3 of the Supplementary Information. The spectra ascertain the existence of sulfur up to a certain film thickness from the surface. These data were collected for the 200 ^{o}C-sulfurized sample.

When considered the XRD, TEM and XPS results, it is proposed that sulfurization driven by the film surface initially induces sulfur incorporation into the oxygen site and, then, incurs the formation of Bi-Fe(III)-Fe(II)-S-O compound and secondary Bi_2S_3 phase with the progress of sulfurization. The Bi-Fe(III)-Fe(II)-S-O compound is likely to be amorphous presumably due to the low processing temperatures. Note that only Bi_2S_3 phase was observed at 400 ^{o}C.
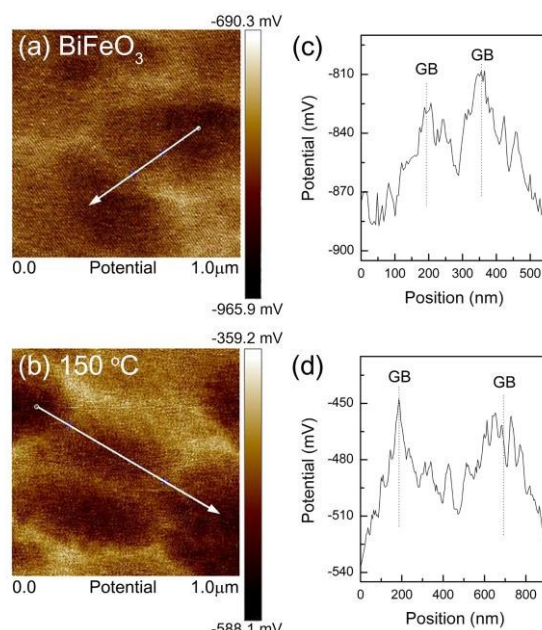
UV-visible transmittance spectra were collected of film samples sulfurized at different temperatures, as well as of a reference sample not subjected to sulfurization. With increasing sulfurization temperature, the transmittance decreased and the absorption edge shifted to longer wavelength (Fig. 5(a)); the differences in transmittance from the fundamental absorption edge varied due to interference arising from the substrate–film and film–air interfaces.[28,29] Plots of $(\alpha h\nu)^2$ versus $h\nu$ were prepared for the unsulfurized and sulfurized films based on their transmittance and reflectance spectra (Fig. 5(b)–(d)). Each film's optical band gap E_g was estimated by extrapolating the linear portion of $(\alpha h\nu)^2$ versus photon energy ($h\nu$), where α is the absorption coefficient. By using the known values of film thickness d, transmittance T and reflectance R, α was calculated from the expression $\alpha=(1/d)\ln[(1-R)^2/T]$. This gave E_g of 2.83 eV for the unsulfurized film, which is very close to the reported value for the BFO thin films.[4,5] The optical band gap of the films significantly decreased as sulfurization progressed: E_g of 2.53 and 1.90 eV were respectively calculated for the samples sulfurized at 150 and 200 °C, in which the BFO phase was still dominant. This substantial reduction in E_g is very promising, and better than or comparable to reported results for cation substitutions.[9-11,30] Thus, it seems that anion substitution is more effective in tuning the band gap. The substantial reduction in E_g after the sulfurization process may be related to the progressive involvement of S followed by phase evolution of Bi_2S_3 phase and Bi-Fe(III)-Fe(II)-S-O compounds as

discussed previously. Bi_2S_3 is known to have a lower band gap of 1.5-1.9 eV.[31]

To gain further insight into potential electrostatic properties across grain boundaries, both unsulfurized and sulfurized BFO thin films grown on FTO/glass were subjected to KPFM measurements. Figs. 6(a) and 6(b) respectively show spatial maps of surface potential on the unsulfurized film and the film sulfurized at 150 °C. Line scans were also conducted, demonstrating distinct peaks in surface potential when the probe moved across grain boundaries (Figs. 6(c)–(d)). That is to say, the grain boundaries were observed to have higher potential than the grain surfaces. This suggests that carrier collection would be enhanced at the grain boundaries of the films. The average grain boundary potentials of the unsulfurized and sulfurized films were measured to be about 50–65 mV and ~85 mV higher than the surface potentials of the grains away from the boundaries. The higher positive charge concentration could be related to the segregation of positively charged O vacancies to the grain boundaries.[32] S at the grain boundary may also contribute to the higher surface potential. With the current knowledge, it is very difficult to explain how the potential Bi-Fe(III)-Fe(II)-S-O compounds can be associated with the enhanced grain boundary potential. At least, S may penetrate into the interior of the film during sulfurization more easily through grain boundaries, because the grain boundary region may provide a more effective diffusion path.[20] Thus, grain boundaries attract electrons, thereby enhancing carrier collection and providing a current pathway for electrons.[33] Band gap narrowing in the BFO thin films with the enhancement in positive surface potential at grain boundaries may improve their applicability for photovoltaic devices.

Conclusions

We have investigated the structures, optical properties and grain boundary potentials of sulfurized BFO films treated at various sulfurization temperatures. According to XRD analysis, the incorporation of S into the perovskite structure seemed to be limited due to the formation of secondary phase of Bi_2S_3, which became dominant above 300 °C. XPS analysis supported well the changed chemical states of the surface of film with the progress of sulfurization, such as increase of the Fe^{2+} oxidation states, involvements of S and the influences of potential defects. Potential formation of complex amorphous Bi-Fe(III)-Fe(II)-S-O compounds was considered. After sulfurization at 150 °C, the band gap of the BFO film was found to decrease from 2.83 to 2.53 eV as a result of anion substitution. The further decrease of the band gap to ~1.90 eV at 200 °C is understood to be directly related to the presence of Bi-Fe(III)-Fe(II)-S-O and Bi_2S_3 phase. The surface potentials at the grain boundaries increased positively with sulfurization progress, suggesting that sulfurization is a promising treatment for the use of BFO in photovoltaic applications.

Acknowledgements

References

1 R. Nechache, C. Harnagea, S. Li, L. Cardenas, W. Huang, J. Chakrabartty, and F. Rosei, *Nat. Photon.*, 2015, **9**, 61-67.
2 R. Nechache, C. Harnagea, S. Licoccia, E. Traversa, A. Ruediger, A. Pignolet, and F. Rosei, *Appl. Phys. Lett.*, 2011, **98**, 202902.
3 B. Chen, Z. Zuo, Y. Liu, Q.-F. Zhan, Y. Xie, H. Yang, G. Dai, Z. Li, G. Xu, and R.-W. Li, *Appl. Phys. Lett.*, 2012, **100**, 173903.
4 W. Ji, K. Yao, and Y. C. Liang, *Adv. Mater.*, 2010, **22**, 1763-1766.
5 X. Chen, H. Zhang, T. Wang, F. Wang, and W. Shi, *Phys. Status Solidi A,* 2012, **209**, 1456-1460.
6 S. R. Basu, L. W. Martin, Y. H. Chu, M. Gajek, R. Ramesh, R. C. Rai, X. Xu, and J. L. Musfeldt, *Appl. Phys. Lett.*, 2008, **92**, 091905.
7 P. Chen, N. J. Podraza, X. S. Xu, A. Melville, E. Vlahos, V. Gopalan, R. Ramesh, D. G. Schlom, and J. L. Musfeldt, *Appl. Phys. Lett.*, 2010, **96**, 131907.
8 H. Dong, Z. Wu, S. Wang, W. Duan, and J. Li, *Appl. Phys. Lett.* 2013, **102**, 072905.
9 X. S. Xu, J. F. Ihlefeld, J. H. Lee, O. K. Ezekoye, E. Vlahos, R. Ramesh, V. Gopalan, X. Q. Pan, D. G. Schlom, and J. L. Musfeldt, *Appl. Phys. Lett.*, 2010, **96**, 192901.
10 L. Peng, H. Deng, J. Tian, Q. Ren, C. Peng, Z. Huang, P. Yang, and J. Chu, *Appl. Surf. Sci.*, 2013, **268**, 146-150.
11 J. Liu, H. Deng, X. Zhai, H. Cao, P. Yang, and J. Chu, *J. Mater. Sci. -Mater. Electron.*, 2015, **26**, 2977-2981.
12 N. Barreau, J.C. Bernede, S. Marsillac, and A. Mokrani, *J. Cryst. Growth,* 2002, **235**, 439-449.
13 A. Ishikawa, T. Takata, J. N. Kondo, M. Hara, H. Kobayashi, and K. Domen, *J. Am. Chem. Soc.*, 2002, **124**, 13547-13553.
14 J. A. Brehm, H. Takenaka, C. W. Lee, I. Grinberg, J. W. Bennett, M. R. Schoenberg, and A. M. Rappe, *Phy. Rev. B*, 2014, **89**, 195202.
15 T. Umebayashi, T. Yamaki, H. Itoh, and K. Asai, *Appl. Phys. Lett.*,2002, **81**, 454.
16 C. S. Jiang, R. Noufi, J. A. AbuShama, K. Ramanathan, H, R. Moutinho, J. Pankow, and M. M. Al-Jassim, *Appl. Phys. Lett.*, 2004, **84**, 3477.
17 C. S. Jiang, R. Noufi, K. Ramanathan, J. A. AbuShama, H. R. Moutinho, and M. M. Al-Jassim, *Appl. Phys. Lett.*, 2004, **85**, 2625.
18 J. C. Lin, R. C. Sharma, and Y. A. Chang, *J. Phase Equilib.*, 1996, **17**, 132-139.
19 J. Keranen, J. Lu, J. Barnard, J. Sterner, J. Kessler, L. Stolt, Th.W. Matthes, E. Olsson, *Thin Solid Films*, 2001, **387**, 80-82.
20 S. M. Lee, and Y. S. Cho, *J. Alloys Compd.* 2013, **579**, 279-283.
21 C. Wang, C. Zhu, T. Zhang, and J. Li, *Vacuum*, 2013, **92**, 7-12.
22 Y. Goushi, H. Hakuma, K. Tabuchi, S. Kijima, K. Kushiya, *Sol. Energy Mater. Sol. Cells*, 2009, **93**, 1318-1320.
23 Z. Quan, H. Hu, S. Xu, W. Liu, G. Fang, M. Li, and X. Zhao, *J, Sol-Gel Sci. Technol.,* 2008, **48**, 261-266.
24 Z. Fang, Y. Liu, Y. Fan, Y. Ni, X. Wei, K. Tang, J. Shen, Y. Chen, *J. Phys. Chem. C*, 2011, **115**, 13968-13976.
25 F. Moulder, W. F. Stickle, P. E. Sobol, and K. D. Bomben, *Handbook of X-Ray Photoelectron Spectroscopy* (Perkin-Elmer, Minnesota, 1992).
26 P. S. V. Mocherla, C. Karthik, R. Ubic, M. S. R. Rao, and C. Sudakar, *Appl. Phys Lett.*, 2013, **103**, 022910.
27 J. Wang, Z. Wang, B. Huang, Y. Ma, Y. Liu, X. Qin, X. Zhang, and Y. Dai, *ACS Appl. Mater. Interfaces*, 2012, **4**, 4024-4030.
28 J. Wu, and J. Wang, *J. Am. Ceram. Soc.*, 2010, **93**, 2795-2803.

29 A. Gaur, P. Singh, N. Choudhary, D. Kumar, M. Shariq, K. Singh, N. Kaur, and D. Kaur, *Physica B*, 2011, **406**, 1877-1882.
30 H. Yan, H. Deng, N. Ding, J. He, L. Peng, L. Sun, P. Yang, and J. Chu, *Mater. Lett*.,2013, **111**, 123-125.
31 V. V. Killedar, S. N. Katore, and C. H. Bhosale, *Mater. Chem. Phys*., 2000, **64**, 166-169.
32 G. Bersuker, D. C. Gilmer, D. Veksler, P. Kirsch, L. Vandelli, A. Padovani, L. Larcher, K. McKenna, A. Shluger, V. Iglesias, M. Porti, and M. Nafría, *J. Appl. Phys*., 2011, **110**, 124518.
33 Y. H. Jo, B. C. Mohanty, D. H. Yeon, S. M. Lee, and Y. S. Cho, *Sol. Energy Mater. Sol. Cells*, 2015, **132**, 136-141.
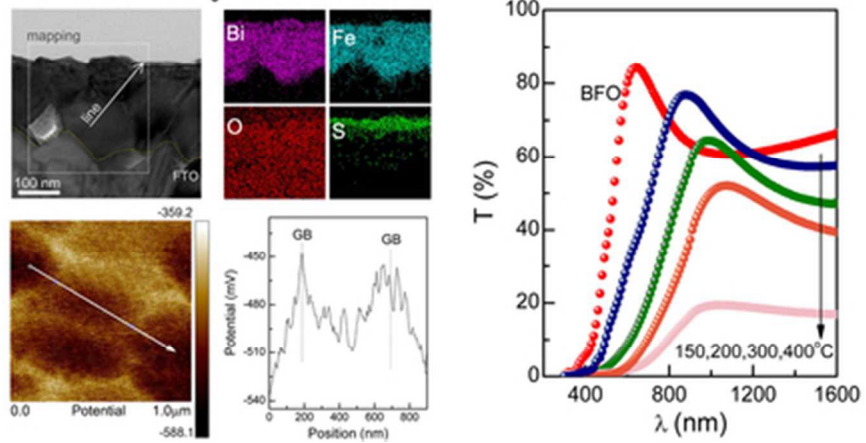
Graphical abstract
39x19mm (300 x 300 DPI)